Cancer Cell International

RESEARCH

Open Access

Potential role of P4HB in the tumor microenvironment and its clinical prognostic value: a comprehensive pan-cancer analysis and experimental validation with a focus on KIRC

Linxue Zhang[1†], Yu-wei Li[2†], Tianyi Xie[3], Ke Sun[1*], Xiang Huang[4*], Wei Xiong[4*] and Rui-ji Liu[4*]

Abstract

Background Tumor microenvironment (TME) plays a crucial role in tumor growth and metastasis. Exploring biomarkers that are significantly associated with TME can help guide individualized treatment of patients.

Methods We analyzed the expression and survival of P4HB in pan-cancer through the TCGA database, and verified the protein level of P4HB by the HPA database. In addition, we used the Metascape database to construct protein–protein interaction networks and the single-cell Sequencing database for functional analysis. An immune cell infiltration analysis was performed to explore the potential role of P4HB in TME. We further analyze the relationship between P4HB and immune checkpoint molecules to explore the role of P4HB in immune checkpoint blockade therapy. Finally, the oncogenic role of P4HB in RCC cells was validated using colony formation and wound healing assays.

Results RNA and protein levels of P4HB were extensively up-regulated in pan-cancer. However, high P4HB expression was associated with poor survival in KIRC. The clinical relevance analyses of P4HB suggested that high P4HB expression was associated with advanced clinical TNM stage. Moreover, multivariate cox regression analysis indicated that P4HB (HR = 1.372, 95% CI 1.047–1.681, $P = 0.019$) was an independent risk factor for OS in KIRC. Functional analysis revealed that P4HB is involved in hypoxia, TME and immune system processes. Our study also found that high P4HB expression was significantly correlated with elevated infiltration levels in CD8 + T cells and M2 macrophages. The results of colony formation and wound healing assays showed that knockdown of P4HB inhibited the RCC growth and migration.

Conclusions P4HB is a specific biomarker for KIRC prognosis and is significantly associated with clinical characteristics. In addition, P4HB may play an influential role in TME and is a biomarker for ICB therapy.

[†]Linxue Zhang and Yu-wei Li have contributed equally to this work.

*Correspondence:
Ke Sun
ksun@uestc.edu.cn
Xiang Huang
billhuang68@163.com
Wei Xiong
37033013@qq.com
Rui-ji Liu
liuruiji66Dr@163.com
Full list of author information is available at the end of the article

Keywords P4HB, Pan-cancer, Tumor microenvironment, Kidney renal clear cell carcinoma, Immune checkpoint molecules

Graphic abstract

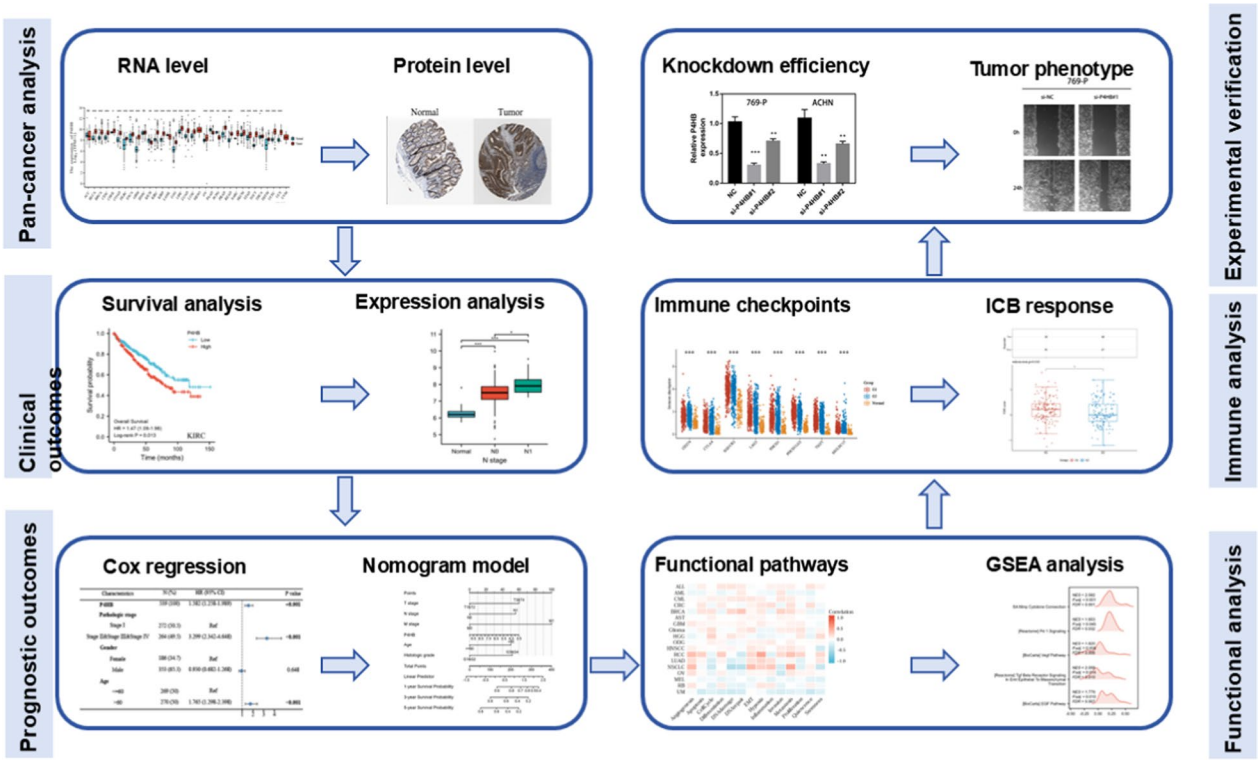

Introduction

Tumor research is changing on a daily basis, shedding light on the mystery of tumorigenesis and malignant biological behavior. Simultaneously, the field of antitumor therapy has experienced significant transformations. The introduction of tamoxifen in the 1970s heralded the era of molecular targeting in cancer treatment. This was followed by the development of gene-targeted therapeutic agents, such as trastuzumab, which were designed based on genetic alterations in tumors and associated signaling pathways. In the realm of tumor immunity and the tumor microenvironment (TME), a range of promising therapeutic approaches has emerged, including immune checkpoint inhibitor antibodies, bispecific T-cell engagers, and chimeric antigen receptor T cells (CAR-T) [1].

Conventional tumor staging (AJCC/TNM) assesses tumor invasion, lymph node metastasis, and distant metastasis [2], offering prognostic value across various cancers [3, 4]. However, it provides limited insights into post-operative outcomes. Patients with the same pathological stage can have varying clinical outcomes: some with advanced disease achieve long progression-free survival (PFS), while around 20% of TNM stage I/II patients face rapid tumor progression or death [5]. This staging system's limitation is its focus on tumor cells, ignoring individual differences in the TME, which evolves with cancer and includes diverse cell types like cancer-associated fibroblasts (CAF), immune cells, and tumor-associated endothelial cells (TEC). The TME is shaped by cells, their secretions, and the vascular network, which reprogram surrounding cells [6]. Immune cells in the TME recognize tumor antigens and generate responses that inhibit tumor growth. CD8+ T cell infiltration in the TME improves prognosis for patients with breast cancer, gastrointestinal stromal tumor, and ovarian cancer [7–9]. Low T-cell infiltration predicts higher recurrence within 5 years for localized cancer, while high T-cell infiltration indicates longer progression-free intervals (PFI) in advanced cancer [10]. Thus, assessing immune cell infiltration in the tumor

microenvironment aids in prognosis and precision therapy.

Prolyl 4-hydroxylase beta polypeptide (P4HB) encodes the beta subunit of proline 4-hydroxylase, belonging to the protein disulfide isomerase family, and is involved in catalyzing disulfide bond formation, breaking, and rearrangement. In a tetramer form, this enzyme is responsible for hydroxylating procollagen residues [11]. Besides acting as a chaperone protein, it also inhibits misfolded protein aggregation in a concentration-dependent manner [12]. Previous research indicates that P4HB promotes breast cancer cell proliferation, migration, and invasion by binding to COL10A1 [13]. In colon cancer cells, P4HB knockdown induces reactive oxygen species, inactivates STAT3 signaling, and leads to cell apoptosis [14]. Additionally, P4HB contributes to chemotherapy resistance in hepatocellular carcinoma via epithelial-mesenchymal transition [15]. However, its prognostic value in pan-cancer and role in the immune microenvironment are still unclear.

In this study, we performed a comprehensive bioinformatics analysis of P4HB in pan-cancer to explore its prognostic value, clinical relevance, functional enrichments, and potential relationship with TME.

Methods and materials

Differential expression of P4HB in pan-cancer analysis

To analyze the differential expression of P4HB in pan-cancer, we used the online tool TIMER 2.0 (http://timer.cistrome.org/) [16]. The Gene_DE module was applied to study the differential expression between tumor and adjacent normal tissues for P4HB across all The Cancer Genome Atlas (TCGA) tumors. A box plot is used to illustrate gene expression levels. In TCGA, tumor tissues such as adrenocortical carcinoma (ACC), acute myeloid leukemia (LAML), etc., have no corresponding adjacent normal tissues. Therefore, we combined UCSC XENA datasets (https://xenabrowser.net/datapages/) and TCGA datasets (https://cancergenome.nih.gov/) for further analysis [17, 18]. The obtained RNAseq data were uniformly processed into transcripts per million reads (TPM) format by the Toil process, and the gene expression data are standardized by $\log_2$ (TPM + 1) [19]. For each tumor differentially expressing P4HB, we performed box plotting using GEPIA2 (http://gepia2.cancer-pku.cn/#index) [20]. Cutoff value is set to $|\mathrm{Log_2FC}| > 1$, P value < 0.05.

TISIDB is a web portal that integrates multiple heterogeneous sources of data about tumors and the immune system (http://cis.hku.hk/TISIDB/index.php) [21]. It can provide literature mining results from PubMed database and other public databases (including UniProt, GO, DrugBank, etc.); High throughput sequencing data on T-cell killing-mediated immune progress; Exome and RNA sequencing data related to immunotherapy, genomics, transcriptomics and clinical data from TCGA. We aim to use TISIDB for molecular subtype analysis of multiple tumor types.

Validation of protein levels in the HPA database

The Human Protein Atlas (HPA, https://www.proteinatlas.org/) is a program initiated in 2003. In this project, cell, tissue, and organ proteins were mapped using a variety of histological techniques such as antibody-based imaging, mass spectrometry-based proteomics, and transcriptomics. In this study, we also validated the protein levels using the HPA database for nine types of tumors differentially expressing P4HB.

Survival analyzes

Clinical data and gene expression data were obtained from the TCGA database. RNAseq data in FPKM (Fregments Per Kilobase per Million) format were standardized by $\log_2$ (FPKM + 1). According to the median of P4HB expression, patients were divided into $\mathrm{P4HB^{high}}$ and $\mathrm{P4HB^{low}}$ groups for overall survival (OS), disease specific survival (DSS) and progress free intervals (PFI) analysis. The log-rank test was used to analyze the survival of patients with different tumors.

Clinical relevance and prognostic role of P4HB in patients with KIRC

In order to understand the clinical relevance of P4HB in kidney renal clear cell carcinoma (KIRC), we evaluated the expression level of P4HB with different clinical characteristics (T, N, M and pathologic stage; histologic grade; age; gender). Furthermore, a receiver operating characteristic curve (ROC) analysis was performed to investigate the predictive ability of P4HB among different clinical features. The area under the curve (AUC) was used to describe the predictive value.

Univariate and multivariate Cox regression analyzes were performed to examine the prognostic significance of P4HB in KIRC. In addition, we combined P4HB and clinical features with Calibration and Nomogram for prognostic analysis to predict 1-year, 3-year, and 5-year survival for KIRC patients.

ScRNA-seq and functional analysis

Single cell RNA sequencing (scRNA-seq) provides an unprecedented opportunity to explore the functional heterogeneity of different types of cancer cells. The CancerSEA database is the first dedicated database for decoding distinct functional states of cancer cells at the single-cell level [22–24]. With 41, 900 cancer single cells in 14 functional states from 25 cancer types, the CancerSEA

database provides an atlas of functional states of cancer single cells. In this study, we used the CancerSEA database with the aim of uncovering which functional states P4HB is associated with at the single-cell level in different cancer types.

The STRING website (https://cn.string-db.org/) was used to analyze the proteins bound to P4HB. The standard settings are as follows: Network type: Full STRING network; required score: low confidence (0.150); Size cutoff: no more than 50 interactors. The 50 proteins that were experimentally verified to bind to P4HB were finally identified. We then input the obtained genes to the Metascape database, a resource for gene annotation and analysis (http://metascape.org/gp/index.html#/main/step1), to construct protein-protein interaction (PPI) networks and perform functional analysis.

Gene set enrichment analysis

A gene set enrichment analysis (GSEA) was conducted to determine the biological pathway differences between groups with higher and lower P4HB levels. A false discovery rate (FDR) of 0.25 and an adjusted *P*-value of 0.05 were used to determine significant pathways. There should be 1000 permutations for each analysis. We visualized GSEA results using the R package "ggplot2".

Tumor microenvironment and immune checkpoint molecules analysis in KIRC

Biologically, renal cell carcinoma differs from other solid tumors that respond to immunotherapy. Therefore, the development of immunotherapies will require an in-depth understanding of disease-specific biology [25]. To investigate the relationship between P4HB expression and immune cell infiltration level and microenvironment in KIRC, we obtained RNA-seq expression (level 3) profiles and corresponding clinical information for KIRC from the TCGA dataset and used CIBERSORT algorithms [26–28] to assess the reliable results of immune score evaluation.

The role of immune checkpoint molecules is to suppress immune cell function and prevent the body from producing an effective anti-tumor immune response, resulting in immune escape of tumors. In this study, we aimed to investigate the differential expression of immune checkpoint-related genes in the $P4HB^{high}$ and $P4HB^{low}$ groups. SIGLEC15, TIGIT, CD274, HAVCR2, PDCD1, CTLA4, LAG3 and PDCD1LG2 are immune checkpoints molecules, and the expression of these eight genes were extracted to observe the expression of immune checkpoint-associated genes. The analysis methods described above were implemented using the ggplot2 and heatmap packages. Immune checkpoint blockade (ICB) therapy has revolutionized the treatment of human cancers [29]. We use the Tumor Immune Dysfunction and Exclusion (TIDE) algorithm [30, 31] to further analysis the effect of different P4HB expression subgroups on predicting the responsiveness of immune checkpoint inhibitors. In recent years, tumor mutational burden (TMB) is of interest in immunotherapy, in concert with PD-L1expression are two important biomarkers for ICB selection across some cancer types [32]. We therefore investigated the relationship between the P4HB expression and the TMB using Spearman's correlation analysis. In addition, we conducted a comprehensive analysis (chemokines, chemokines receptors and immunostimulators) to completely understand the role of P4HB in immunotherapy response using TISIDB datasets.

Analysis of molecular targeted therapies

There is a poor prognosis for metastatic clear cell renal cell carcinomas (mccRCCs) and targeted therapy as the first-line treatment option can provide a survival benefit [33]. According to the largest publicly available pharmacogenomic database Cancer Drug Sensitivity Genomics (GDSC, https://www.cancerrxgene.org/), chemotherapeutic response for each sample is predicted based on the KIRC transcriptome. We applied half-maximal inhibitory concentration (IC50) to assess the relationship between sample treatment response and P4HB expression. The prediction process was implemented by the R package "pRRophetic". Ridge regression was used to estimate IC50 for the KIRC sample.

Cell culture and transfection

The HK-2 and RCC cell lines were obtained from the American Type Culture Collection (Manassas, VA, USA) and cultured in Dulbecco's modifed Eagle's medium (DMEM; gibco) with 10% foetal bovine serum (FBS, Gibco) and 1% penicillin/streptomycin at 37 °C in a 5% CO_2 atmosphere. Cells were transfected with siRNA-P4HB#1, #2 and NC using jetPRIME® transfection reagent (NY, USA) when cell density reached about 60%. These siRNAs and relevant NC were designed by GenePharma (Shanghai, China).

RNA isolation and RT-qPCR

Total RNA was extracted using RNAeasyTM (Beyotime; Shanghai, China) according to the manufacturer's instruction. We used HiScript® II reverse transcriptase (Vazyme; Nanjing, China) to convert RNA to cDNA and performed RT-qPCR with LineGene 9600 Plus (Bioer Technology, Hangzhou, China) using 2×SYBR Green qPCR Master Mix (High ROX; Servicebio; Wuhan, China). The expression of P4HB were normalized to GAPDH, and relative expression was calculated using the $2^{-\Delta\Delta}$ Ct method [34].

Western blotting

Briefly, protein lysates were extracted with RIPA and quantified using BCA kits. Equal protein amounts were separated by 6–12% SDS-PAGE and transferred to PVDF membranes. After blocking, membranes were incubated overnight with primary antibodies (P4HB, CSB-PA00254A0Rb; GAPDH, AF1186) at 4 °C and then with secondary antibodies for 2 h at room temperature. Bands were visualized using the Bio-Rad ChemiDoc XRS.

Immunofluorescence assay and immunohistochemistry (IHC)

Tissues from human RCC were fixed, embedded, and sectioned. After drying at 60 °C for 2 h, sections underwent IHC staining. Slides were incubated overnight at 4 °C with a primary antibody (CSB-PA00254A0Rb, CUSABIO; Wuhan, China), then with a secondary antibody for one hour at room temperature. After DAB visualization, slides were counterstained with hematoxylin, dehydrated in alcohol, cleared in xylene, and mounted with Permount for microscopy.

Colony formation assay

After transfection, cells were plated in a six-well plate at a density of 1×10^3 cells per well and incubated for 2 weeks at 37 °C in a 5% CO_2 atmosphere. Following cell culture, cells were washed with PBS, fixed with 4% paraformaldehyde, stained with 0.1% crystal violet, and observed for colonies with a diameter > 0.1 mm under a microscope [35].

Wound healing assay

Briefly, cells were seeded in six-well plates and a scratch was made when cell density was close to 90%. Wound healing was observed and photographed after 0 and 24 h. The wound closure rate was measured three times and averaged [36].

Statistics analysis

R foundation for statistical computing (2020) version 4.0.3 was used for graphing and statistical analysis. The statistical differences between the two groups were compared by the Wilcoxon test and the significance differences between the three groups were tested by the Kruskal-Wallis test. A Bonferroni correction method was used for the effects of multiple hypothesis testing (Dunn's test, P. adj < 0.05). $P < 0.05$ is considered statistically significant.

Results

Differential expression of P4HB in pan-cancer analysis

TIMER 2.0 was used to analyze the differential expression of P4HB in pan-cancer. As shown in Fig. 1a, the expression of P4HB was upregulated in Bladder Urothelial carcinoma (BLCA), Breast invasive carcinoma (BRCA), Cervical squamous cell carcinoma and endocervical adenocarcinoma (CESC), Cholangiocarcinoma (CHOL), Colon adenocarcinoma (COAD), Esophageal carcinoma (ESCA), Glioblastoma multiforme (GBM), Head and Neck squamous cell carcinoma (HNSC), KIRC, Liver hepatocellular carcinoma (LIHC), Lung adenocarcinoma (LUAD), Lung squamous cell carcinoma (LUSC), Prostate adenocarcinoma (PRAD), Rectum adenocarcinoma (READ), Uterine Corpus Endometrial carcinoma (UCEC) compared to the corresponding adjacent normal tissues. The results of combined UCSC XENA datasets and TCGA datasets further validated the aberrant expression of P4HB in pan-cancer (Fig. 1b). To investigate the relationship between P4HB expression and molecular subtypes in each tumor, we performed an online analysis with TISIDB. In Fig. 1c, elevated P4HB expression is significantly correlated with HM-indel status in COAD and HER-2 status in BRCA tumors.

For tumors (COAD, UCEC, PRAD, BRCA, LUSC, BLCA, LIHC, KIRC, LUAD) differentially expressing P4HB, we performed box plotting using GEPIA2 (Fig. 2). Subsequently, the protein expression level of P4HB was verified by the HPA database. Most of the cancers showed moderate immunoreactivity. Liver, colon, kidney and endometrial cancers showed strong staining in several cases. Testicular cancer, gliomas and lymphomas were negative or weakly stained in a majority of cases (Fig. 2). Immunohistochemical staining showed that P4HB protein was mainly located in the cytoplasm or cell membrane of the cells.

Survival analysis of P4HB expression in pan-cancer

To investigate the prognostic value of P4HB in pan-cancer, we performed a comprehensive survival analysis. KIRC patients with elevated expression of P4HB had poorer OS, DSS and PFI than those with low expression. In addition, BLCA patients with high expression of P4HB had poorer PFI. However, COAD patients with high expression of P4HB had better DFS compared to the group with low expression of P4HB (Fig. 3, Figs. S1, S2). In summary, P4HB may be a potentially specific prognostic biomarker for patients with KIRC.

Clinical relevance and prognostic role of P4HB in patients with KIRC

The baseline characteristics of KIRC patients in TCGA based on P4HB expression are summarized in Table 1. In KIRC patients, high expression of P4HB was strongly associated with advanced T-stage, positive lymph nodes, distant metastases, advanced TNM stage, and advanced histological stage. However, no obvious correlation

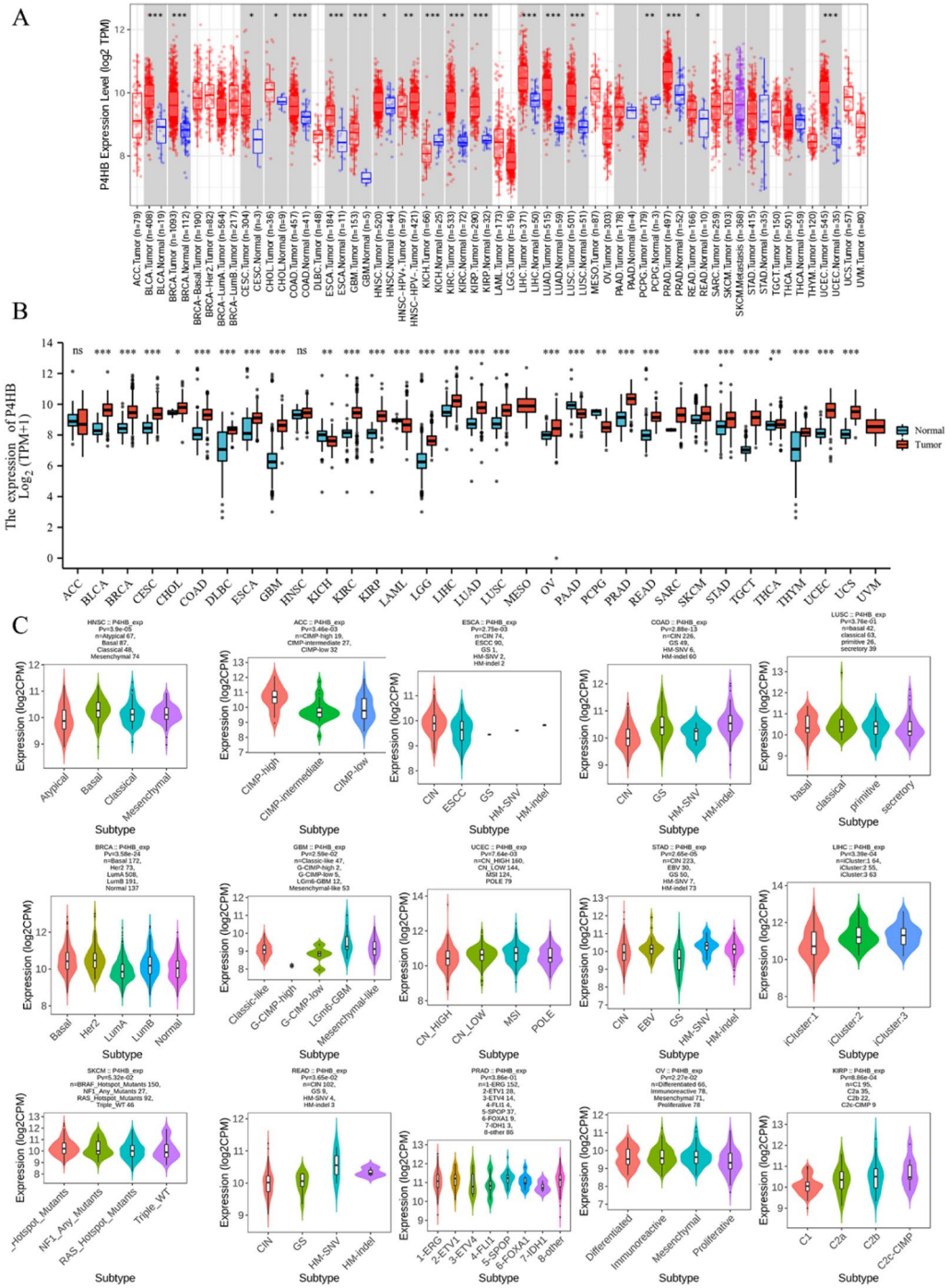

Fig. 1 RNA expression levels of P4HB in pan-cancer. **a** Differential expression of P4HB across all TCGA tumors between the tumor and adjacent normal tissue. **b** Differential expression analysis between tumor and normal tissues using UCSC XENA dataset and TCGA dataset. **c** Molecular subtype analysis of multiple tumor types using TISIDB. *$P < 0.05$, **$P < 0.01$, ***$P < 0.001$

between P4HB expression and the age and gender of KIRC patients were observed (Fig. 4a–g). Subsequently, we performed ROC analysis to investigate the diagnostic value of P4HB expression at T, N, M, TNM, histological stage and tumor status. The results showed that P4HB had good diagnostic value for tumor status (AUC = 0.951 95% CI 0.927–0.975). It also had diagnostic value for positive lymph nodes (AUC = 0.728 95% CI 0.610–0.846) (Fig. S3).

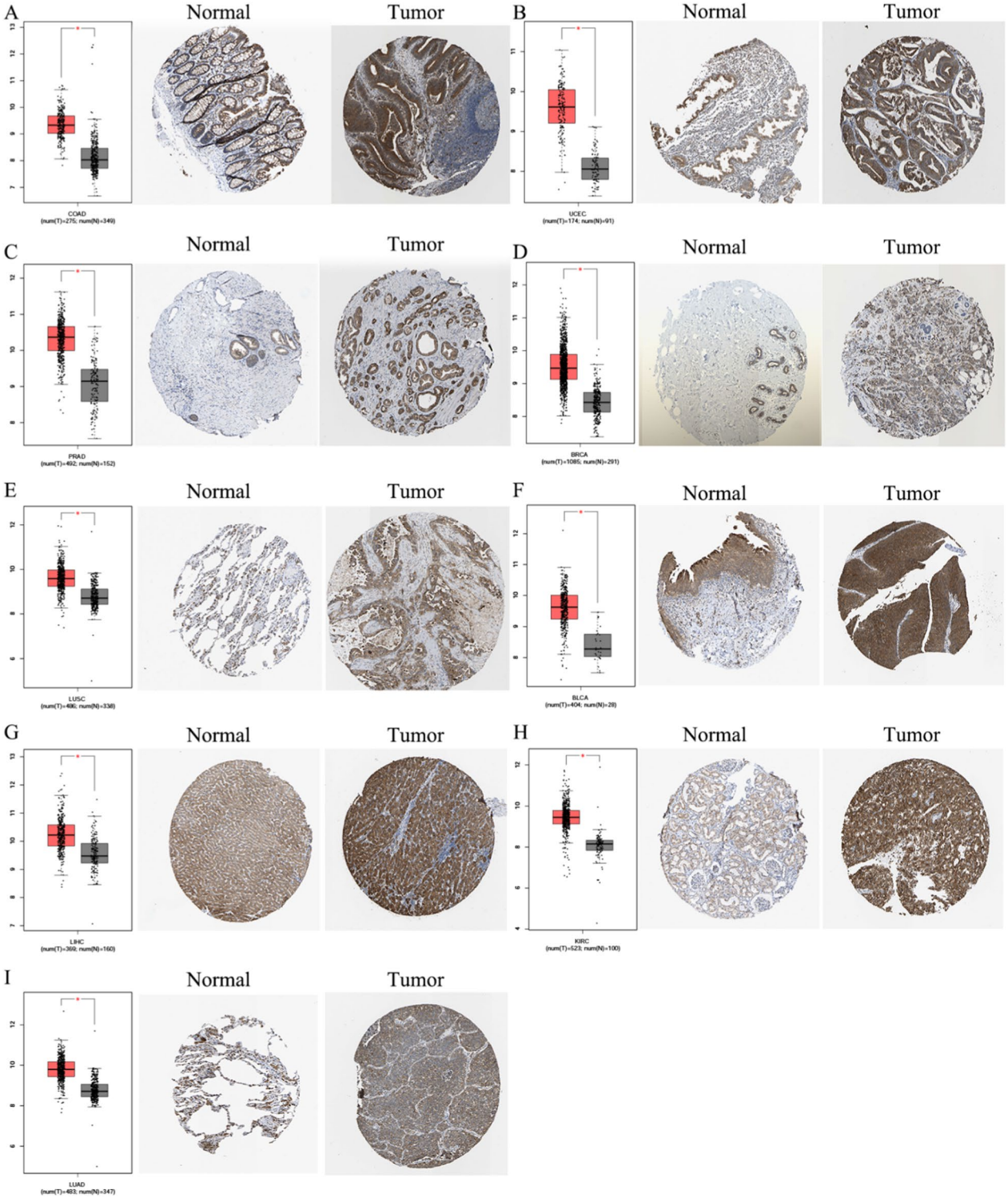

Fig. 2 P4HB protein expression levels in tumors with differential expression of P4HB. **a–i** Box plots (left) demonstrated the RNA level of tumors differentially expressing P4HB using GEPIA2. Cutoff value is set to $|Log_2FC| > 1$, *P* value < 0.05. The HPA database was used to analyze the protein expression level (right) of P4HB in **a** COAD; **b** UCEC; **c** PRAD; **d** BRCA; **e** LUSC; **f** BLCA; **g** LIHC; **h** KIRC; **i** LUAD. **P* < 0.05

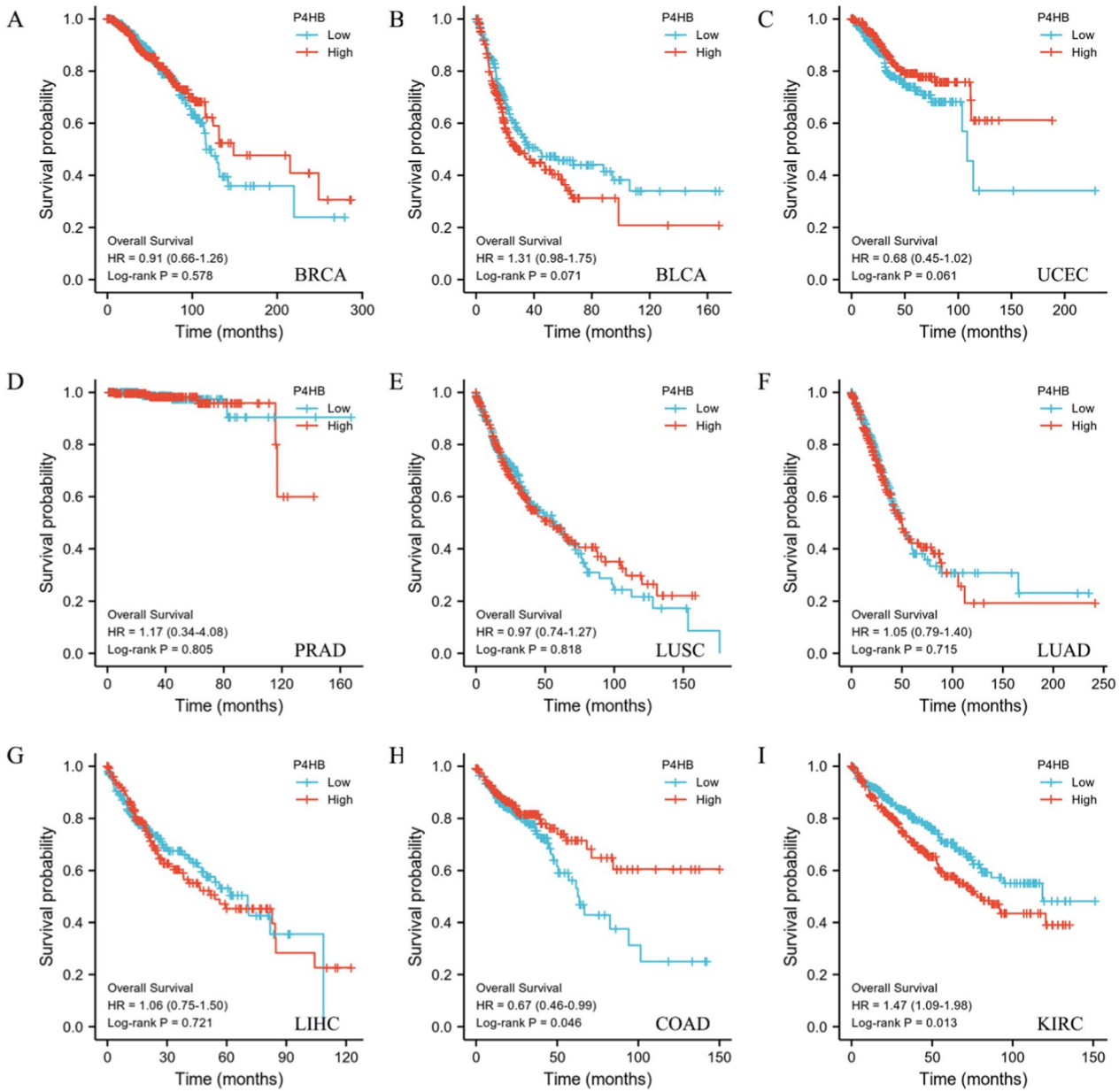

Fig. 3 Overall survival analysis of P4HB in tumors. **a–i** Survival analysis comparing P4HB high and P4HB low expression groups in **a** BRCA; **b** BLCA; **c** UCEC; **d** PRAD; **e** LUSC; **f** LUAD; **g** LIHC; **h** COAD; **i** KIRC. The survival outcomes were analyzed using the log-rank test

To explore the risk factors involved in the prognosis of KIRC patients, we performed a univariate Cox regression analysis on the expression of P4HB, as well as other clinical variables. As shown in Fig. 4h, P4HB (HR = 1.582, 95% CI 1.258–1.989, $P < 0.001$), TNM stage (HR = 3.299, 95% CI 2.342–4.648, $P < 0.001$) and age (HR = 1.765, 95% CI 1.298–2.398, $P < 0.001$) are risk factors for OS in patients with KIRC.

Furthermore, we performed multivariate Cox regression analysis and found that P4HB (HR = 1.372, 95% CI 1.047–1.681, $P = 0.019$) was an independent risk factor for OS (Table 2). Based on the results of multivariate cox regression analysis, we integrated multiple clinical variables and plotted the Nomogram (Fig. 4i). We use the calibration curve to assess the difference between the predicted and true values of this Cox regression model. As shown in Fig. 4j, the predicted 3-year and 5-year survival probabilities for this model are close to the true survival probabilities, suggesting that this Nomogram model has clinical prognostic value.

Table 1 Baseline characteristics of KIRC patients in TCGA according to P4HB expression

Characteristic	Low expression of P4HB	High expression of P4HB	*P* value
N	269	270	
T stage, n (%)			0.014
T1	155 (28.8%)	123 (22.8%)	
T2	36 (6.7%)	35 (6.5%)	
T3	75 (13.9%)	104 (19.3%)	
T4	3 (0.6%)	8 (1.5%)	
N stage, n (%)			0.043
N0	116 (45.1%)	125 (48.6%)	
N1	3 (1.2%)	13 (5.1%)	
M stage, n (%)			0.008
M0	221 (43.7%)	207 (40.9%)	
M1	27 (5.3%)	51 (10.1%)	
Pathologic stage, n (%)			0.003
Stage I	154 (28.7%)	118 (22%)	
Stage II	32 (6%)	27 (5%)	
Stage III	52 (9.7%)	71 (13.2%)	
Stage IV	30 (5.6%)	52 (9.7%)	
Histologic grade, n (%)			< 0.001
G1	13 (2.4%)	1 (0.2%)	
G2	144 (27.1%)	91 (17.1%)	
G3	87 (16.4%)	120 (22.6%)	
G4	19 (3.6%)	56 (10.5%)	
Gender, n (%)			0.628
Female	96 (17.8%)	90 (16.7%)	
Male	173 (32.1%)	180 (33.4%)	
Age, median (IQR)	60 (51, 68)	61.5 (52, 72)	0.058

ScRNA-seq, functional analysis, and gene set enrichment of P4HB

We applied CancerSEA to explore which functional states P4HB is associated with in pan-cancer at single-cell resolution. Figure 5a is a heatmap of the 14 different functional states of P4HB involved in pan-cancer. The results showed that P4HB was associated with a variety of malignant biological processes, such as being involved in regulating hypoxic processes in renal cell carcinoma (RCC); promoting distant metastasis in non-small cell lung cancer (NSCLC); and mediating DNA repair in BRCA. Figure 5b, c list 10 biological processes in which P4HB is involved in RCC. In addition to hypoxic processes ($r = 0.678$, $P < 0.001$), P4HB also regulates angiogenesis ($r = 0.517$, $P < 0.001$), regulates differentiation ($r = 0.432$, $P < 0.001$), stemness ($r = 0.411$, $P < 0.001$), promotes proliferation ($r = 0.340$, $P = 0.002$) and metastasis ($r = 0.403$, $P < 0.001$) in RCC. However, P4HB expression was negatively correlated with cell cycle ($r = -0.271$, $P = 0.013$), DNA repair ($r = -0.427$, $P < 0.001$) and inflammation ($r = -0.359$, $P < 0.001$) in RCC.

We obtained 50 proteins from the STRING database with experimentally validated binding to P4HB and constructed a PPI network (Fig. 6a). Additionally, we used the Metascape database for functional annotation of P4HB related genes and constructed network components (Fig. 6b–d). The Molecular Complex Detection (MCODE) algorithm has been applied to identify densely connected network components. Component 1 is mainly enriched in "protein folding", "response to endoplasmic reticulum stress" and "protein processing in endoplasmic reticulum". Component 2 is involved in "hydroxylation of the molecule". Component 4 participate in "organelle biogenesis and maintenance". Component 5 regulates "processing of intronless pre-mRNAs", "processing of capped intronless pre-mRNA" and "mRNA polyadenylation". Figure 6e lists the top-level Gene Ontology biological processes associated with the P4HB related genes. Interestingly, these genes are enriched mainly in cellular processes, metabolic processes, biological regulation, and immune system processes.

Figure 7A–D presents the results of GSEA. The results demonstrated that the gene sets were mainly enriched in oncogenic signaling pathways, such as P53 pathway; PTEN pathway; MTOR pathway. Similar to the results of scRNA-seq, the association between P4HB and hypoxia signaling pathway (HIF pathway) was also obtained in this analysis. P4HB gene set was also enriched in cytokines and immune response pathways, such as IL-6 pathway; MMP cytokine connection; sumoylation of immune response proteins. Metabolism-related signaling pathways were also found in this analysis: fatty acid metabolism; glycolysis and iron metabolism. Interestingly, PD-1 pathway and VEGF pathway were enriched in this analysis which indicated that P4HB may be a potential biomarker for ICB or molecular-targeted therapies in KIRC patients

Tumor microenvironment and immune checkpoint molecules analysis in KIRC

We aimed to investigate whether P4HB is involved in the tumor microenvironment to regulate the malignancy progression of KIRC. CIBERSORT was used to analyze the immune cell infiltration of KIRC in different P4HB expression groups (Fig. 8a–c). B cells, macrophages and T cells are the main immune infiltrating cells in KIRC (Fig. 8b). The goal of tumor immunotherapy is to activate cytotoxic T lymphocytes (CTLS) in tumors, initiate tumor-specific CTLS in lymphoid organs, and establish an effective immune response to tumors [26]. An important function of CD8+ and CD4+ T cells is to optimize the size and quality of the CTL response and provide

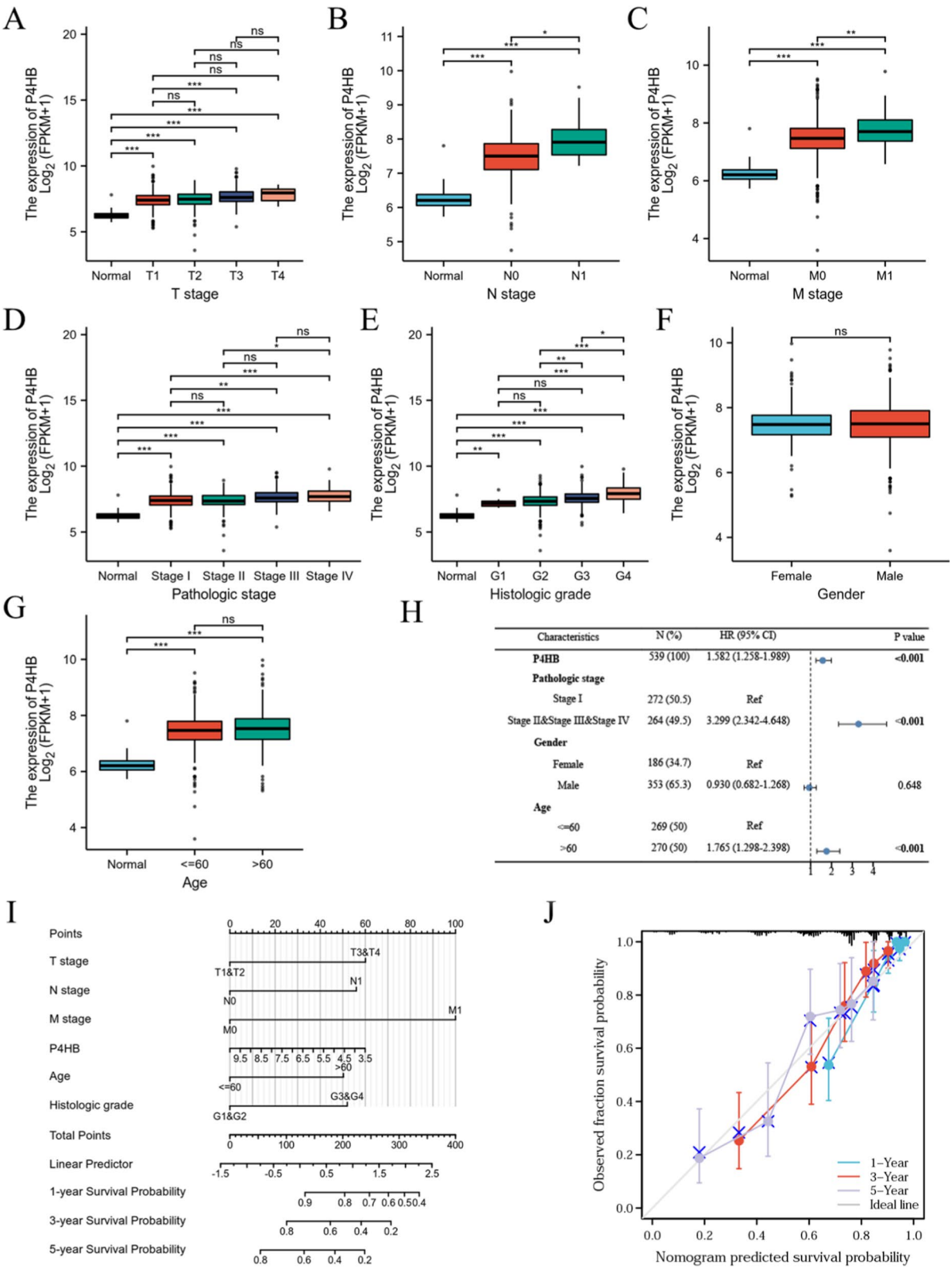

Fig. 4 Clinical relevance and prognostic role of P4HB in KIRC patients. **a–g** Box plots of P4HB expression between T stages (**a**); N stages (**b**); M stages (**c**); pathological stages (**d**); histologic stages (**e**); gender (**f**); age (**g**). **h** Univariate Cox regression analysis of P4HB in KIRC. Prognostic model was constructed using Nomogram (**i**) and verified by Calibration (**j**). n.s, not significant, *$P < 0.05$, **$P < 0.01$, ***$P < 0.001$

Table 2 Univariate and multivariate cox regression analyses on the expression of P4HB and other clinical variables in KIRC

Characteristics	Total (N)	Univariate analysis		Multivariate analysis	
		Hazard ratio (95% CI)	*P* value	Hazard ratio (95% CI)	*P* value
P4HB	539	1.582 (1.258–1.989)	<0.001	1.327 (1.047–1.681)	0.019
Gender	539				
Female	186	Reference			
Male	353	0.930 (0.682–1.268)	0.648		
Age	539				
<=60	269	Reference			
>60	270	1.765 (1.298–2.398)	<0.001	1.648 (1.211–2.243)	0.001
Pathologic stage	536				
Stage I	272	Reference			
Stage II & III & IV	264	3.299 (2.342–4.648)	<0.001	3.036 (2.145–4.297)	<0.001

a long-term protective immunity [37]. Interestingly, CD8+ T cell infiltration levels were lower in the high P4HB expression group than in the low P4HB expression group (Fig. 8c). Macrophages play a crucial role in cancer development and metastasis. Compared to proinflammatory M1 macrophages which phagocytose tumor cells, anti-inflammatory M2 macrophages, including tumor-associated macrophages (TAMs), promote tumor growth [38]. In this study, we found that high expression of P4HB was significantly associated with higher levels of M2 macrophage infiltration (Fig. 8c). In summary, P4HB is involved in the regulation of the microenvironment of KIRC. Overexpression of P4HB promotes tumorigenesis by up-regulating the infiltration levels of M2 macrophages and down-regulating the infiltration levels of CD8+T cells, resulting in tumor immune escape.

Cancer therapy has been revolutionized by discovering that overexpression of immune checkpoint molecules in TME plays a crucial role in antitumor immune evasion [39]. Therefore, understanding the relationship between P4HB and immune checkpoint molecules is conducive to exploring the potential mechanisms of P4HB in regulating the TME. In this study, higher expression of P4HB in KIRC was significantly associated with higher expression of immune checkpoint molecules HAVCR2 and PDCD1LG2 compared to lower expression of P4HB. However, no obvious association between P4HB and CD274 (PD-L1) or CTLA4 was found (Fig. 8d, e). Therefore, we hypothesize that P4HB promotes tumor immune escape through immunosuppression induced by the overexpression of HAVCR2 and PDCD1LG2 on T cells.

To further explore the association between P4HB expression level and immune checkpoint blockade (ICB) response in KIRC, we performed tumor mutational burden analysis. There was a positive correlation between P4HB expression and TMB score in the results (Fig. 9a). Furthermore, we analyzed the response to ICB treatment in the P4HB high and low expression groups and found that the P4HB high expression group had a higher response to ICB treatment (Fig. 9b). In addition, we also conducted a comprehensive analysis (chemokines, chemokine receptors and immunostimulators) to thoroughly understand the role of P4HB in immunotherapy response and found that P4HB was positively correlated with CXCR6, CXCL16 and CD70 (Fig S4a-f). It has been reported that CXCR6 and CXCL16 to be involved in the efficacy of anti-PD-1 cancer immune checkpoint therapy [40], and CD70 is an effective target for chimeric antigen receptor T (CAR-T) cell therapy [41].

Analysis of molecular-targeted therapies

Molecular targeted therapy is the first-line treatment for advanced renal cell carcinoma. Studying the expression of P4HB and IC50 for molecularly targeted therapeutics may help guide clinical treatment strategies. The IC50 of sorafenib, sunitinib, axitinib, imatinib, pazopanib, and erlotinib decreased with the increase of P4HB expression (Fig. 10a–f). It is worth noting that P4HB expression was significantly correlated with the IC50 of sorafenib ($r = -0.34$, $P < 0.001$). The results suggest that KIRC patients with high expression of P4HB can derive better drug sensitivity from molecularly targeted therapies, suggesting P4HB as a potential biomarker for molecularly targeted therapy selection.

P4HB promotes the proliferation and migration of RCC cells

We validated the expression level of P4HB in RCC cells and found that P4HB was highly expressed in ACHN and 769-P cells (Fig. 11a). To further explore the role of P4HB in RCC cell proliferation and migration, we transfected siRNA into ACHN and 769-P cells and finally decided to

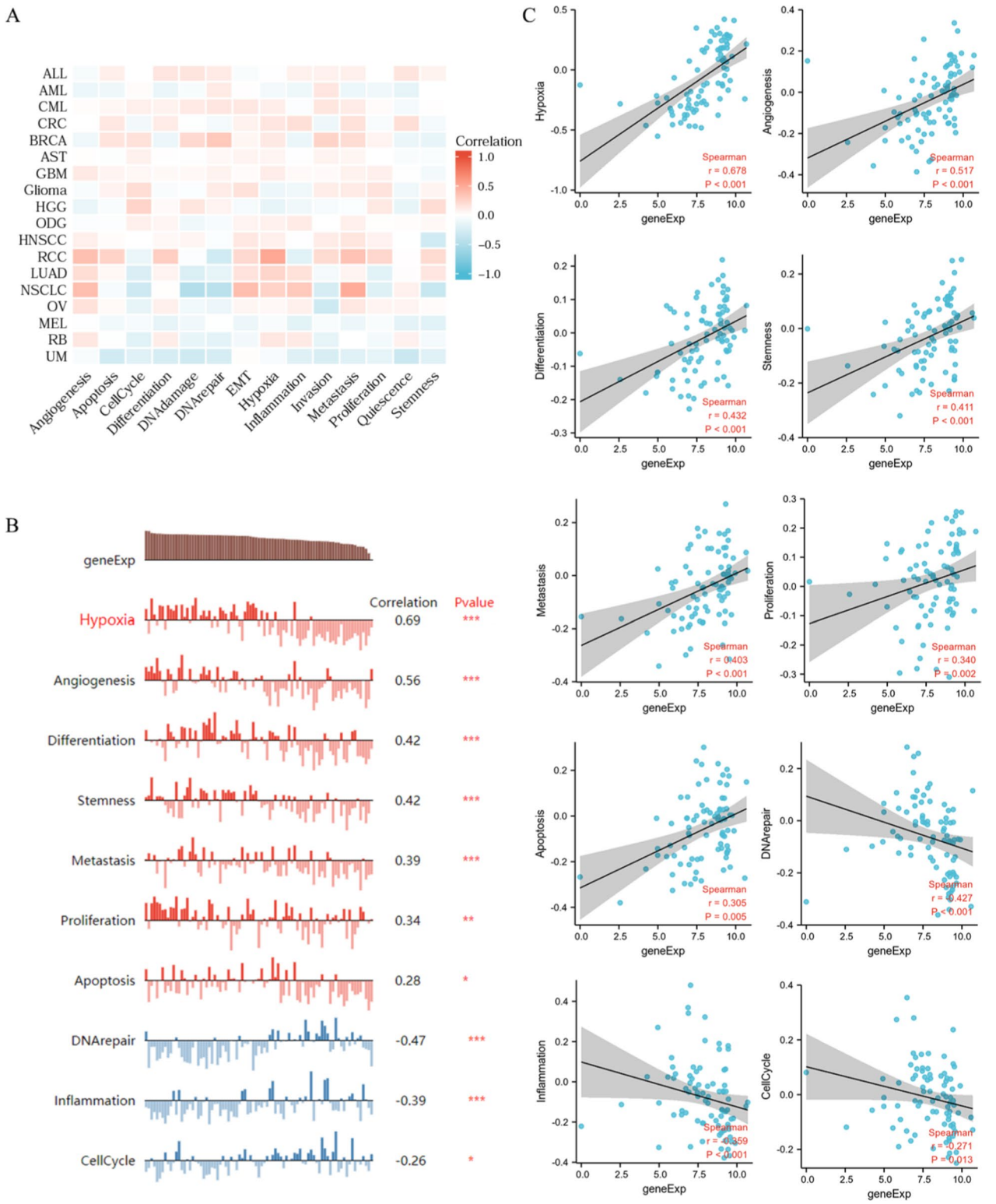

Fig. 5 ScRNA-seq and functional analysis. **a** Heatmap of the P4HB functional pathways in pan-cancer. **b** Relationship between P4HB expression and the top 10 enriched pathways in KIRC. **c** Spearman's method was used to assess the correlation between P4HB expression and enrichment pathways. *$P < 0.05$, **$P < 0.01$, ***$P < 0.001$

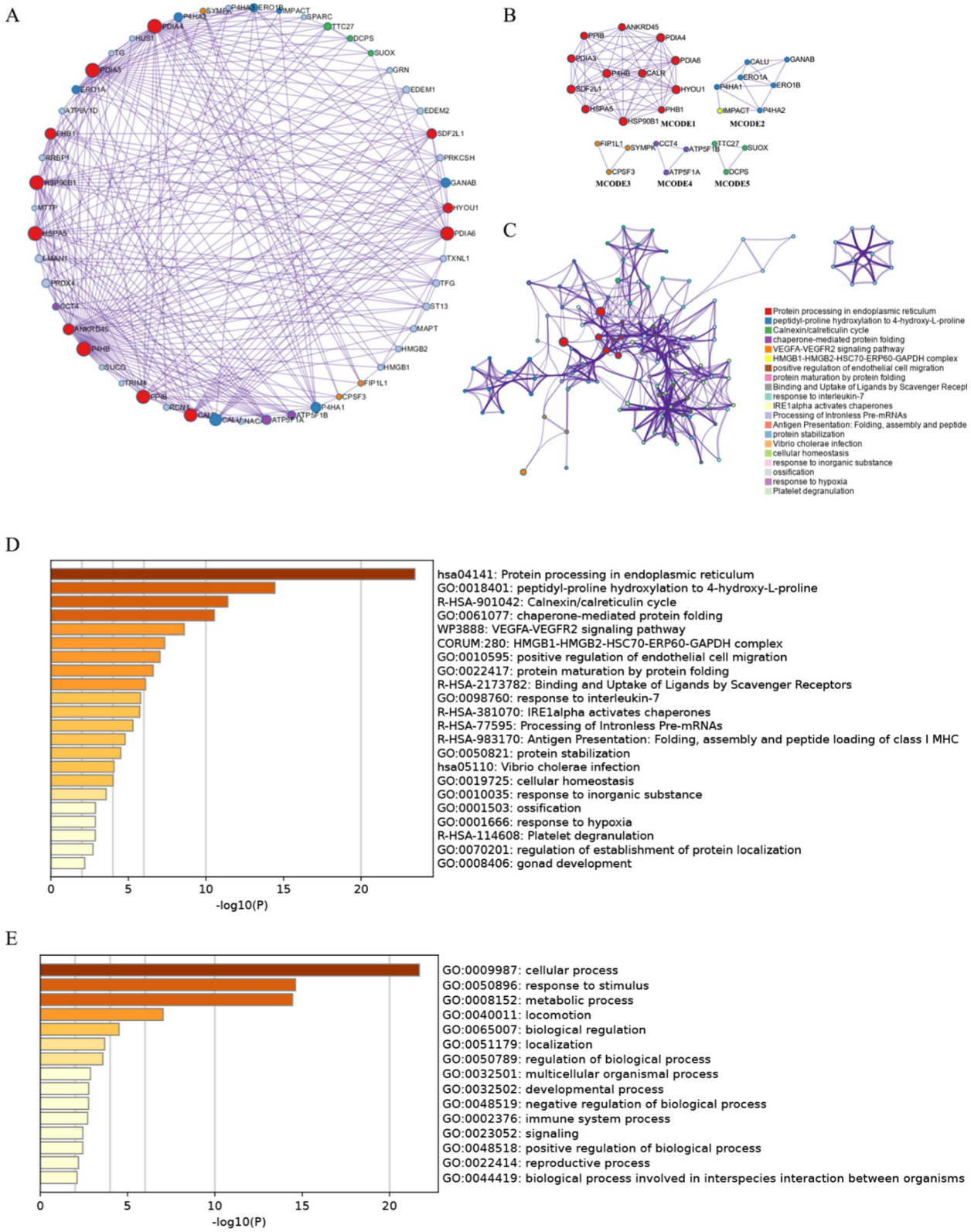

Fig. 6 PPI networks and Gene Ontology analysis. **a** The PPI network is constructed by the STRING database with 50 proteins which were experimentally verified binding to P4HB. **b** Densely connected network components had been identified by Molecular Complex Detection algorithm (MCODE). **c, d** Constructed network components (**c**) and functional annotation (**d**) of P4HB related genes using Metascape database. **e** Top-level Gene Ontology biological processes associated with P4HB-related genes

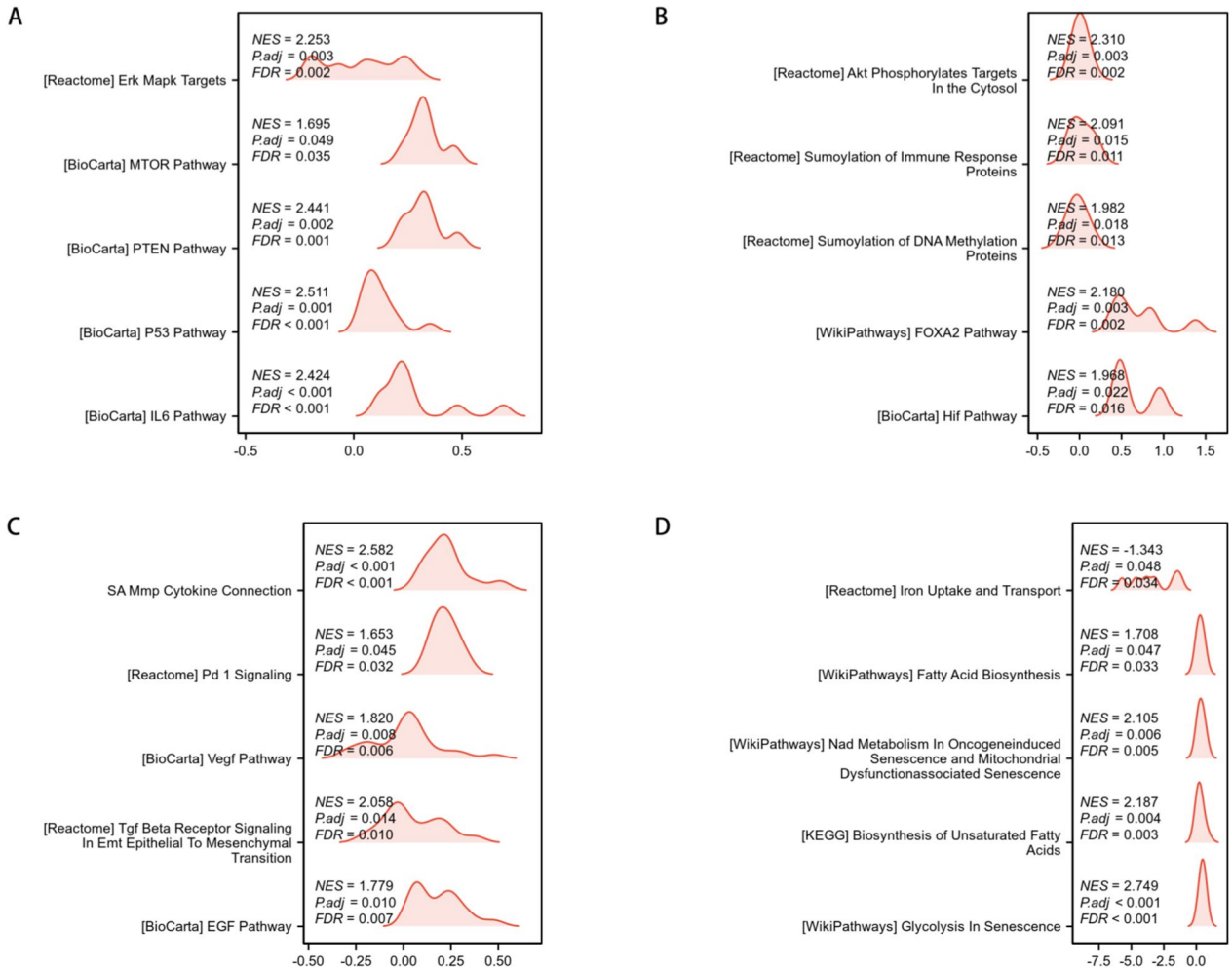

Fig. 7 GSEA functional enrichment analysis of P4HB expression in KIRC (**a–d**). The Y-axis represents one gene set and the X-axis is the distribution of log FC corresponding to the core molecules in each gene set

take the next step with si-P4HB#1(Fig. 11b, Fig. S5a). The results showed that knockdown of P4HB inhibited the proliferation and migration of RCC cells (Fig. 11c–f). In addition, we further performed IHC analysis on clinical RCC tissues and found that P4HB expression was significantly higher in RCC than in paracancer tissues (Fig S5b).

Discussion

A prior study using TCGA and Gene Expression Omnibus (GEO) databases found elevated P4HB levels in BLCA, confirmed by qPCR and western blot, and identified P4HB as an independent risk factor for poor OS in BLCA [42]. Our pan-cancer analysis also shows widespread up-regulation of P4HB, indicating its potential oncogenic role in tumor development. We discovered that high P4HB expression is linked to unfavorable molecular subtypes in COAD and BRCA, indicating its role in tumor cell differentiation. For instance, Zhang et al. noted increased P4HB in HER-2 positive breast tumors, potentially boosting metabolic, stress response, and antioxidant activities in the tumor microenvironment [43]. We investigated P4HB's prognostic value in pan-cancer and found that high P4HB expression in KIRC patients correlated with poorer OS, DSS, and PFI, unlike other tumor types. This led us to examine its clinical relevance in KIRC, revealing significant associations with greater tumor invasion (T), positive lymph nodes (N), distant metastases (M), advanced stage, and poor differentiation (G). In addition, P4HB is an independent risk factor for OS in KIRC patients. Therefore,

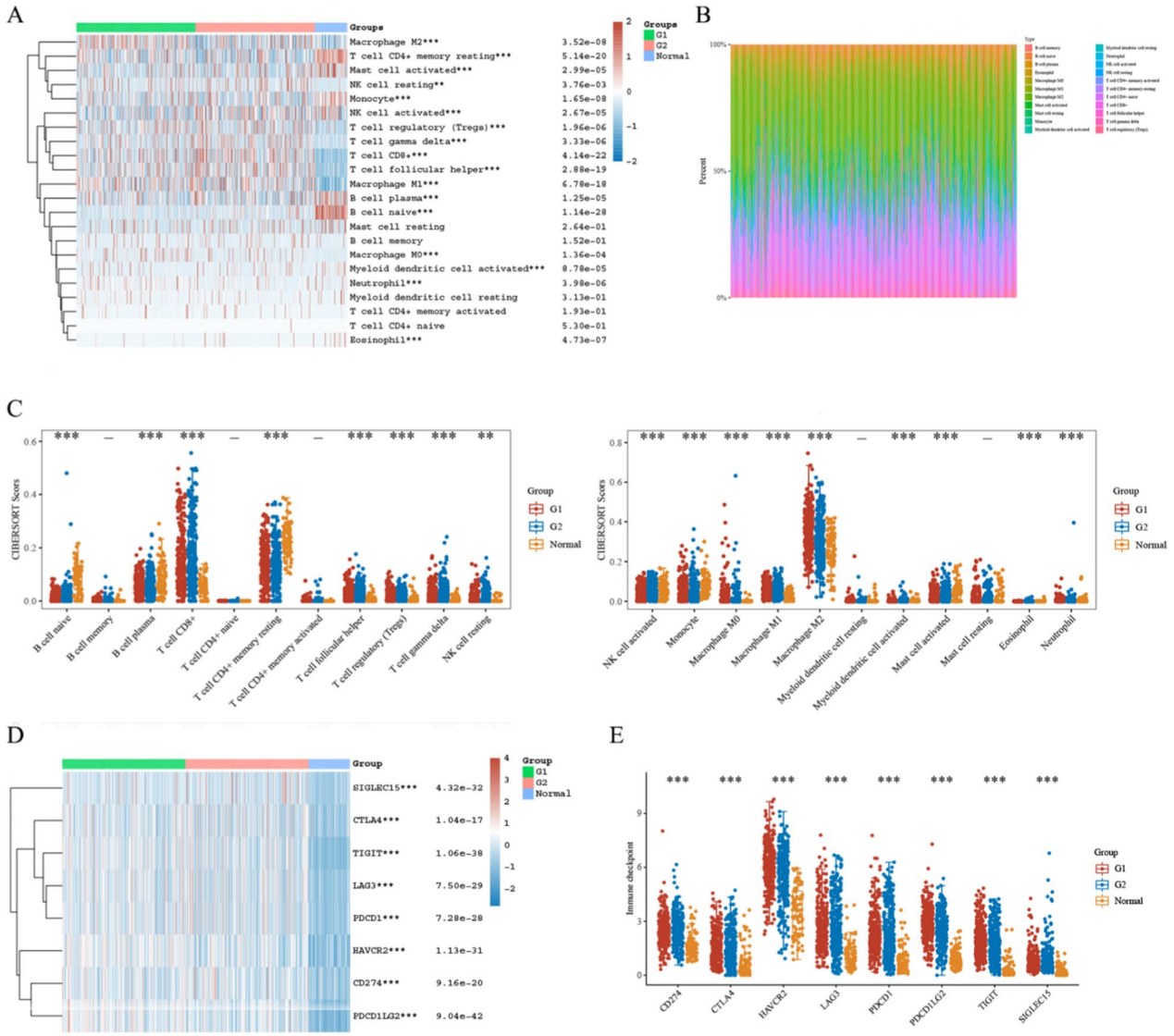

Fig. 8 P4HB expression and tumor microenvironment analysis in KIRC. **a** Immune cell score heatmap, different colors represent different expression distribution in different samples. **b** Percentage abundance of tumor infiltrating immune cells in each sample. Different colors represent different types of immune cells. The abscissa represents the sample, and the ordinate represents the percentage of immune cell content in a single sample. **c** Box plots of immune cell score using CIBERSORT. **d** Heatmap of immune-checkpoint-related gene expression. The different colors represent the trend of gene expression in different samples. **e** Expression distribution of immune checkpoints gene in tumor tissues and normal tissues. G1, P4HB high group; G2 P4HB low group. *$P < 0.05$, **$P < 0.01$, ***$P < 0.001$

we suggest that P4HB may be a specific prognostic biomarker in KIRC.

We analyzed scRNA-seq and GSEA to examine P4HB's role in KIRC, finding it potentially promotes RCC progression through hypoxia, immune microenvironment, tumor metabolism, cell differentiation, proliferation, apoptosis, and metastasis. Wang et al. found that inhibiting P4HB in bladder cancer increased gemcitabine sensitivity and enhanced its anti-tumor effects by promoting apoptosis [44]. P4HB, a target gene of HIF-1α, plays a role in the hypoxic microenvironment of gastric cancer, aiding in cell invasion and metastasis [45]. In diffuse gliomas, high P4HB expression correlates with frequent TP53 mutations, promotes glioma cell proliferation, and its inhibition enhances chemotherapy and radiotherapy effectiveness [46].

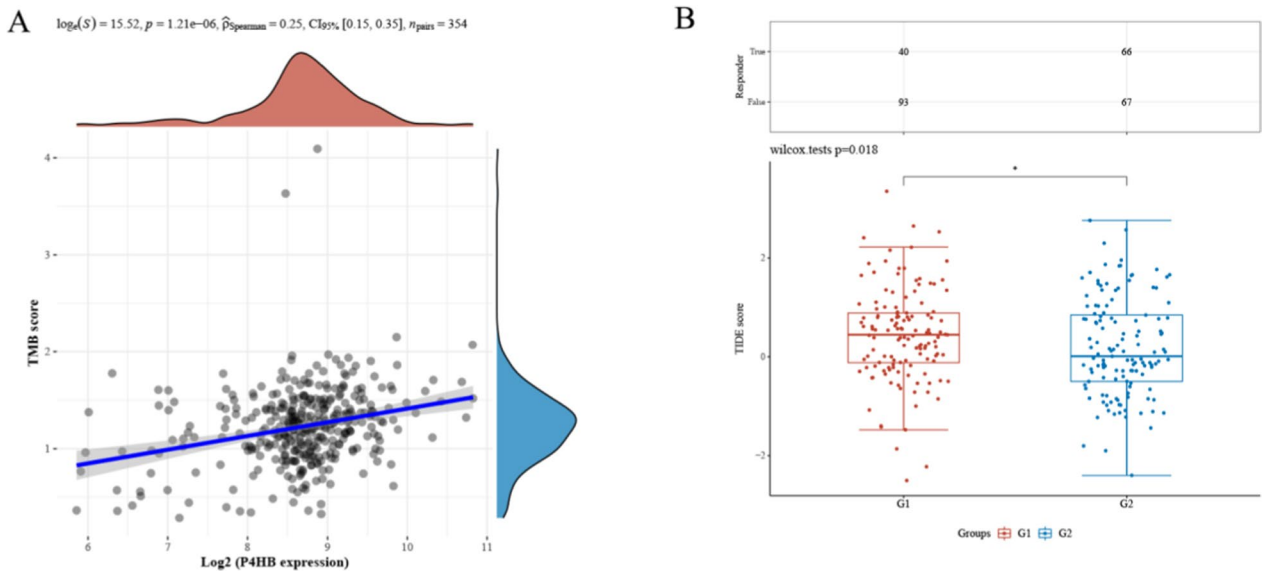

Fig. 9 TMB and ICB analysis of P4HB in KIRC. **a** Correlation analysis between P4HB gene expression and TMB was performed using the Spearman's method. **b** Statistical table of immune response of samples in different groups in the prediction results (above). The distribution of immune response scores in different groups in the prediction results (below). G1, P4HB high group; G2 P4HB low group. *$P < 0.05$

Previous studies have investigated immune microenvironment-related biomarkers (e.g., STON1 [47], ARPC1B [48]) in KIRC and found that the expression of these genes was significantly correlated with immunotherapy response [49]. In our GO analysis, we discovered P4HB's involvement in immune processes, prompting us to investigate its role in the TME. Systematic analysis in KIRC revealed that high P4HB expression correlates with low CD8+ T cell infiltration and high M2 macrophage levels. Microenvironment changes drive macrophage differentiation into inflammatory (M1) or regulatory (M2) subtypes based on cytokine stimuli [50]. In tumors, M2 macrophages are the main component and increase as the tumor grows, releasing molecules like VEGF, EGF, and TGFβ to promote growth and metastasis [38]. T cells, divided into CD4+ and CD8+ subsets, play a crucial role, with high CD8+ T cell infiltration being a positive prognostic indicator [51–53]. This study also found a positive correlation between P4HB expression and CXCR6 and CXCL16. Interestingly, CXCR6 and CXCL16 were demonstrated to be involved in M2 polarization of macrophages [54].

T cells recognize pathogens by binding their T-cell receptor (TCR) to the peptide-major histocompatibility complex (MHC) of target cells. Immune checkpoints, which include co-stimulating and co-inhibiting receptors and ligands, regulate this interaction [55]. When antigen/MHC binds to co-inhibitory receptors on T cells, activation is inhibited. This study found that HAVCR2 and PDCD1LG2 expression levels were significantly higher in the high P4HB expression group compared to the low P4HB expression group. HAVCR2 (also known as T cell immunoglobulin and mucin domain containing 3, TIM3) molecule expression on T cells depleted in the context of chronic viral infection and tumor. For example, clonal accumulation dysfunctional CD8+ T cells overexpressing HAVCR2 promotes immune escape of leukemic cells [56]. In addition, T cells expressing high levels of PD-1 and HAVCR2 co-inhibitors appeared to be more numerous than dysfunctional T cells expressing PD-1 alone, implying a favorable clinical value of combined blockade of PD-1 and HAVCR2 in the future [57]. PDCD1LG2 (PD-L2) is the second B7 homolog that binds PD-1. It is the common receptor of PD-1 with PD-L1 and participates in the immunosuppression of T cells by blocking cell cycle progression [58]. In KIRC patients, P4HB expression increases synergistically with immune checkpoint molecules, and high expression groups can achieve larger responses to ICB therapy, suggesting P4HB as a potential biomarker for ICB therapy.

Conclusion

P4HB is highly upregulated in various cancers and serves as a specific prognostic biomarker for KIRC. Its expression is closely linked to clinical features of KIRC patients and independently predicts poor overall survival.

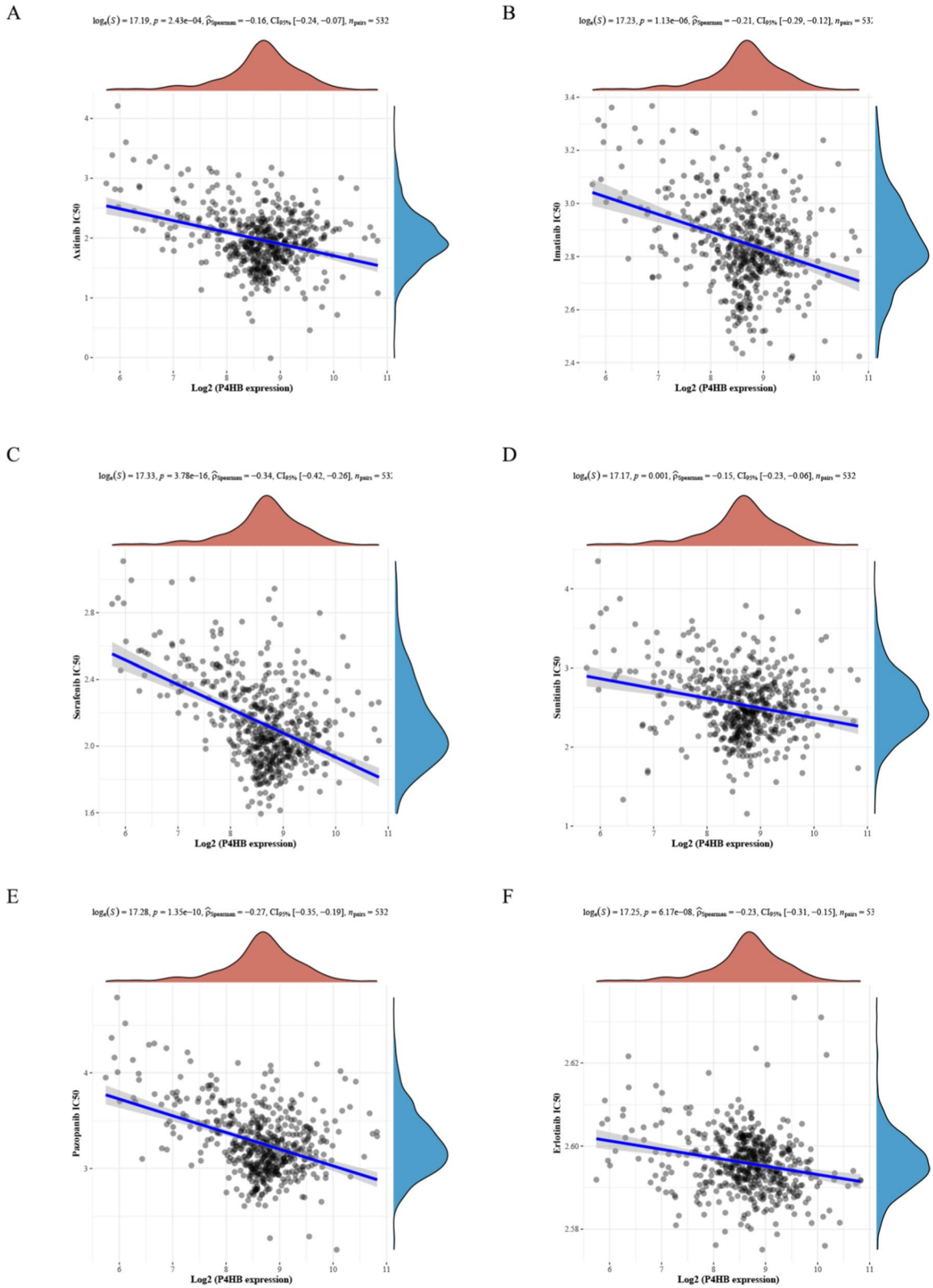

Fig. 10 Molecular targeted therapy analysis in KIRC. **a–f** Spearman correlation analysis of P4HB gene expression and IC50 score **a** Axitinib; **b** Imatinib; **c** Sorafenib; **d** Sunitinib; **e** Pazopanib; **f** Erlotinib. The abscissa represents different groups of samples, and the ordinate represents the distribution of the IC50 score. The density curve on the right represents the trend in distribution of the IC50 score, the upper density curve represents the trend in distribution of the gene expression

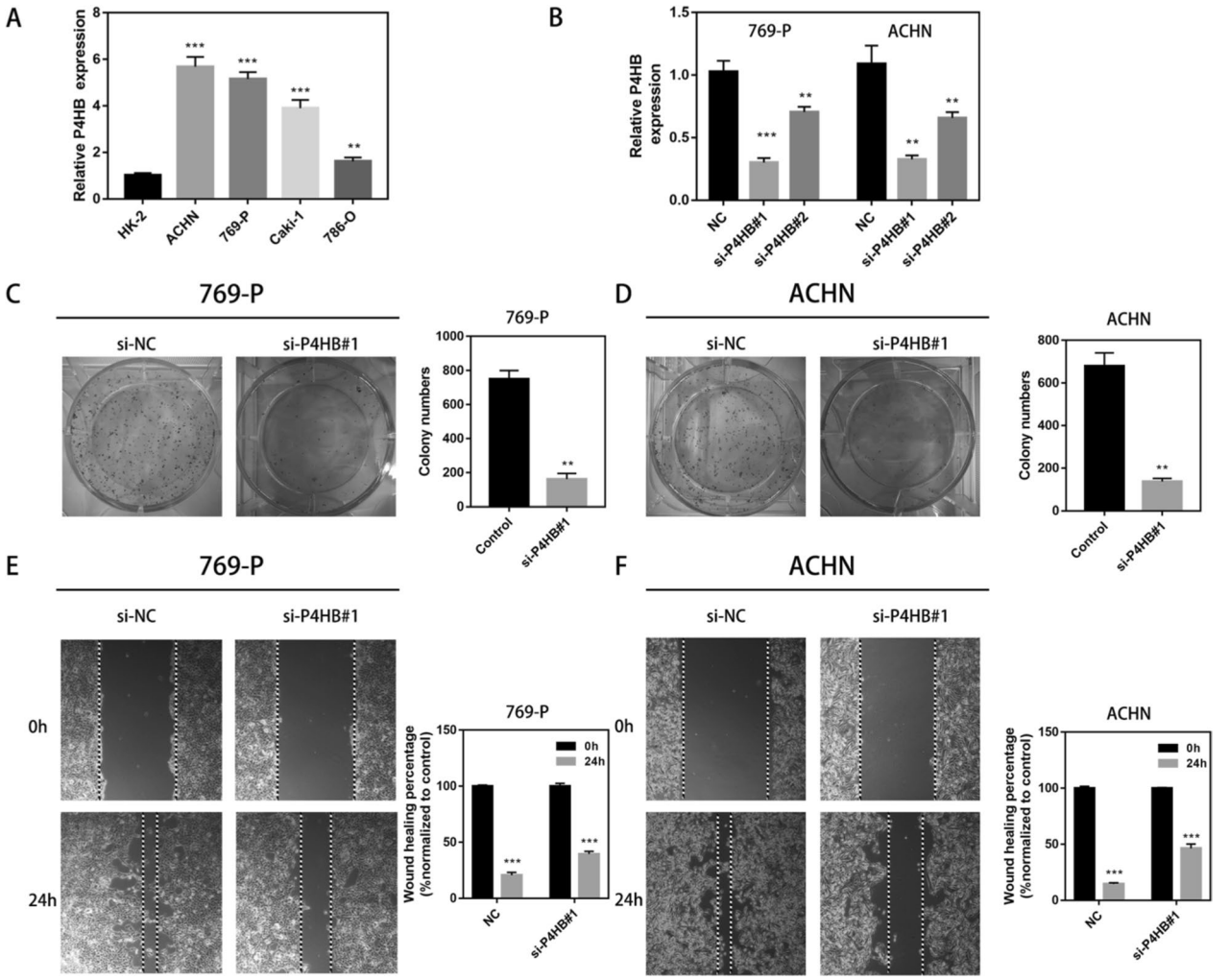

Fig. 11 Knockdown of P4HB inhibits cell proliferation and migration of 769-P and ACHN. **a** P4HB expression was examined in HK-2 and RCC cells lines via quantitative reverse transcription polymerase chain reaction (RT qPCR); **b** Efficiencies of P4HB inhibition was examined by RT qPCR; **c, d** The effects of P4HB inhibition on cell proliferation were detected by clone formation in 769-P cell (**c**) and ACHN cell (**d**); **e, f** The effects of P4HB knockdown on migration were observed in769-P (**e**) and ACHN cell (**f**) by wound healing assays

Additionally, P4HB levels correlate with CD8+ T cell and M2 macrophage infiltration in the tumor microenvironment and indicate response to ICB therapy.

Abbreviations

TME	Tumor microenvironment
TCGA	The Cancer Genome Atlas
GEO	Gene Expression Omnibus
RCC	Renal cell carcinoma
KIRC	Kidney renal clear cell carcinoma
ICB	Immune checkpoint blockade
PFS	Progression-free survival
TAMs	Tumor-associated macrophages
CAF	Cancer-associated fibroblasts
TEC	Tumor-associated endothelial cell
PFI	Progression-free intervals
P4HB	Prolyl 4-hydroxylase beta polypeptide
OS	Overall survival
DSS	Disease specific survival
ROC	Operating characteristic curve
AUC	Area under the curve
ScRNA-seq	Single cell RNA sequencing
GSEA	Gene set enrichment analysis
FDR	False discovery rate
mccRCCs	Metastatic clear cell renal cell carcinomas
IC50	Half-maximal inhibitory concentration
BLCA	Bladder Urothelial carcinoma
BRCA	Breast invasive carcinoma
CESC	Cervical squamous cell carcinoma and endocervical adenocarcinoma
CESC	Cholangiocarcinoma
COAD	Colon adenocarcinoma
ESCA	Esophageal carcinoma
GBM	Glioblastoma multiforme
HNSC	Head and Neck squamous cell carcinoma
LIHC	Liver hepatocellular carcinoma
LUAD	Lung adenocarcinoma
LUSC	Lung squamous cell carcinoma
PRAD	Prostate adenocarcinoma
READ	Rectum adenocarcinoma
UCEC	Uterine Corpus Endometrial carcinoma

HR	Hazard ratio
CI	Confidence interval

Supplementary Information

The online version contains supplementary material available at https://doi.org/10.1186/s12935-024-03575-z.

Additional file 1.

Acknowledgements
We thank all the authors for the support in this study.

Author contributions
RJL designed this study. RJL, LXZ and YWL conducted data extraction, analysis. RJL, LXZ, YWL, TYX, KS and XH wrote the manuscript. RJL, KS, WX and XH reviewed and revised the manuscript.

Funding
This study was funded by The Research Fund of Sichuan Academy of Medical Sciences and Sichuan Provincial People's Hospital (No.2023BH13).

Availability of data and materials
No datasets were generated or analysed during the current study.

Declarations

Ethics approval and consent to participate
The studies complied with local laws and institutional guidelines. Written informed consent was not needed from participants or their legal guardians/next of kin, as per national legislation and institutional requirements.

Consent for publication
The final manuscript was read and approved by all authors.

Competing interests
The authors declare no competing interests.

Author details
[1]School of Materials and Energy, University of Electronic Science and Technology of China, Chengdu 610054, China. [2]School of Medicine, University of Electronic Science and Technology of China, Chengdu 610054, Sichuan, China. [3]Department of Neuroscience, Kenneth P. Dietrich School of Arts & Science, University of Pittsburgh, Pittsburgh, PA, USA. [4]Department of Urology, Sichuan Provincial People's Hospital, School of Medicine, University of Electronic Science and Technology of China, Chengdu 610072, China.

Received: 3 July 2024 Accepted: 13 November 2024
Published online: 03 January 2025

References

1. Sonkin D, Thomas A, Teicher BA. Cancer treatments: Past, present, and future. Cancer Genet. 2024;286–287:18–24.
2. Galon J, Pagès F, Marincola FM, Angell HK, et al. Cancer classification using the Immunoscore: A worldwide task force. J Transl Med. 2012;10:205.
3. Weitz J, Koch M, Debus J, Höhler T, et al. Colorectal cancer. Lancet. 2005;365(9454):153–65.
4. Locker GY, Hamilton S, Harris J, Jessup JM, et al. ASCO 2006 update of recommendations for the use of tumor markers in gastrointestinal cancer. J Clin Oncol. 2006;24(33):5313–27.
5. Mlecnik B, Bindea G, Pagès F, Galon J. Tumor immunosurveillance in human cancers. Cancer Metastasis Rev. 2011;30(1):5–12.
6. Wu T, Dai Y. Tumor microenvironment and therapeutic response. Cancer Lett. 2017;387:61–8.
7. Mahmoud SM, Paish E, Powe DG, Macmillan RD, et al. Tumor-infiltrating CD8+ lymphocytes predict clinical outcome in breast cancer. J Clin Oncol. 2011;29(15):1949–55.
8. Zhang L, Conejo-Garcia J, Katsaros D, Gimotty PA, et al. Intratumoral T cells, recurrence, and survival in epithelial ovarian cancer. N Engl J Med. 2003;348(3):203–13.
9. Rusakiewicz S, Semeraro M, Sarabi M, Desbois M, et al. Immune infiltrates are prognostic factors in localized gastrointestinal stromal tumors. Cancer Res. 2013;73(12):3499–510.
10. Mlecnik B, Tosolini M, Kirilovsky A, Berger A, et al. Histopathologic-based prognostic factors of colorectal cancers are associated with the state of the local immune reaction. J Clin Oncol. 2011;29(6):610–8.
11. Vuori K, Pihlajaniemi T, Marttila M, Kivirikko KI, et al. Characterization of the human prolyl 4-hydroxylase tetramer and its multifunctional protein disulfide-isomerase subunit synthesized in a baculovirus expression system. Proc Natl Acad Sci U S A. 1992;89(16):7467–70.
12. Noiva R. Protein disulfide isomerase: the multifunctional redox chaperone of the endoplasmic reticulum. Semin Cell Dev Biol. 1999;10(5):481–93.
13. Yang W, Wu X, Zhou F. Collagen type X alpha 1 (COL10A1) contributes to cell proliferation, migration, and invasion by targeting prolyl 4-hydroxylase beta polypeptide (P4HB) in breast cancer. Med Sci Monit. 2021;27:e928919.
14. Zhou Y, Yang J, Zhang Q, et al. P4HB knockdown induces human HT29 colon cancer cell apoptosis through the generation of reactive oxygen species and inactivation of STAT3 signaling. Mol Med Rep. 2019;19(1):231–7.
15. Ma X, Wang J, Zhuang J, et al. P4HB modulates epithelial-mesenchymal transition and the β-catenin/Snail pathway influencing chemoresistance in liver cancer cells. Oncol Lett. 2020;20(1):257–65.
16. Li T, Fu J, Zeng Z, et al. TIMER2.0 for analysis of tumor-infiltrating immune cells. Nucleic Acids Res. 2020;48(W1):W509–14.
17. Liu H, Weng J. A pan-cancer bioinformatic analysis of RAD51 regarding the values for diagnosis, prognosis, and therapeutic prediction. Front Oncol. 2022;12: 858756.
18. Liu H, Dilger JP, Lin J. A pan-cancer-bioinformatic-based literature review of TRPM7 in cancers. Pharmacol Ther. 2022;240: 108302.
19. Vivian J, Rao AA, Nothaft FA, et al. Toil enables reproducible, open source, big biomedical data analyses. Nat Biotechnol. 2017;35(4):314–6.
20. Tang Z, Li C, Kang B, et al. GEPIA: a web server for cancer and normal gene expression profiling and interactive analyses. Nucleic Acids Res. 2017;45(W1):W98–102.
21. Ru B, Wong CN, Tong Y, et al. TISIDB: an integrated repository portal for tumor-immune system interactions. Bioinformatics. 2019;35(20):4200–2.
22. Yuan H, Yan M, Zhang G, et al. CancerSEA: a cancer single-cell state atlas. Nucleic Acids Res. 2019;47(D1):D900–8.
23. Cao K, Ling X, Jiang X, et al. Pan-cancer analysis of UBE2T with a focus on prognostic and immunological roles in lung adenocarcinoma. Respir Res. 2022;23(1):306.
24. Yu L, Ding Y, Wan T, et al. Significance of CD47 and its association with tumor Immune microenvironment heterogeneity in ovarian cancer. Front Immunol. 2021;12: 768115.
25. Braun DA-O, Bakouny Z, Hirsch L, et al. Beyond conventional immune-checkpoint inhibition - novel immunotherapies for renal cell carcinoma. Nat Rev Clin Oncol. 2021;18(4):199–214.
26. Newman AM, Liu CL, Green MA-O, et al. Robust enumeration of cell subsets from tissue expression profiles. Nat Methods. 2015;12(5):453–7.
27. Gentles AJ, Newman AM, Liu CL, et al. The prognostic landscape of genes and infiltrating immune cells across human cancers. Nat Med. 2015;21(8):938–45.
28. Bai R, Yin P, Xing Z, et al. Investigation of GPR143 as a promising novel marker for the progression of skin cutaneous melanoma through bioinformatic analyses and cell experiments. Apoptosis. 2024;29(3–4):372–92.
29. Morad G, Helmink BA, Sharma P, et al. Hallmarks of response, resistance, and toxicity to immune checkpoint blockade. Cell. 2021;184(21):5309–37.
30. Jiang PA-O, Gu S, Pan D, et al. Signatures of T cell dysfunction and exclusion predict cancer immunotherapy response. Nat Med. 2018;24(10):1550–8.
31. Wang T, Guo K, Zhang D, et al. Disulfidptosis classification of hepatocellular carcinoma reveals correlation with clinical prognosis and immune profile. Int Immunopharmacol. 2023;120: 110368.
32. Chan TA, Yarchoan M, Jaffee E, et al. Development of tumor mutation burden as an immunotherapy biomarker: utility for the oncology clinic. Ann Oncol. 2019;30(1):44–56.

33. Hsieh JJ, Purdue MP, Signoretti S, et al. Renal cell carcinoma. Nat Rev Dis Primers. 2017;3:17009.
34. Liu RJ, Xu ZP, Huang X, et al. Yin Yang 1 promotes the neuroendocrine differentiation of prostate cancer cells via the non-canonical WNT pathway (FYN/STAT3). Clin Transl Med. 2023;13(10): e1422.
35. Wan L, Liu Y, Liu R, et al. GAD1 contributes to the progression and drug resistance in castration resistant prostate cancer. Cancer Cell Int. 2023;23(1):255.
36. Liu RJ, Xu ZP, Li SY, et al. BAP1-related ceRNA (NEAT1/miR-10a-5p/SERPINE1) promotes proliferation and migration of kidney cancer cells. Front Oncol. 2022;12: 852515.
37. Reina-Campos M, Scharping NE, Goldrath AA-OX. CD8(+) T cell metabolism in infection and cancer. Nat Rev Immunol. 2021;21(11):718–38.
38. Xia Y, Rao L, Yao H, et al. Engineering macrophages for cancer immunotherapy and drug delivery. Adv Mater. 2020;32(40): e2002054.
39. Barroso-Sousa R, Barry WT, Garrido-Castro AC, et al. Incidence of endocrine dysfunction following the use of different immune checkpoint inhibitor regimens: A systematic review and meta-analysis. JAMA Oncol. 2018;4(2):173–82.
40. Di Pilato M, Kfuri-Rubens R, Pruessmann JN, et al. CXCR6 positions cytotoxic T cells to receive critical survival signals in the tumor microenvironment. Cell. 2021;184(17):4512–30.
41. Ji F, Zhang F, Zhang M, et al. Targeting the DNA damage response enhances CD70 CAR-T cell therapy for renal carcinoma by activating the cGAS-STING pathway. J Hematol Oncol. 2021;14(1):152.
42. Wu Y, Peng Y, Guan B, et al. P4HB: A novel diagnostic and prognostic biomarker for bladder carcinoma. Oncol Lett. 2021;21(2):95.
43. Zhang D, Tai LK, Wong LL, Chiu L-L, et al. Proteomic study reveals that proteins involved in metabolic and detoxification pathways are highly expressed in HER-2/neu-positive breast cancer. Mol Cell Proteomics. 2005;4(11):1686–96.
44. Wang X, Bai YA-O, Zhang F, et al. Targeted inhibition of P4HB promotes cell sensitivity to gemcitabine in urothelial carcinoma of the bladder. Onco Targets Ther. 2020;13:9543–58.
45. Zhang J, Guo S, Wu Y, et al. P4HB, a novel hypoxia target gene related to gastric cancer invasion and metastasis. Biomed Res Int. 2019;2019:9749751.
46. Zou H, Wen C, Peng Z, et al. P4HB and PDIA3 are associated with tumor progression and therapeutic outcome of diffuse gliomas. Oncol Rep. 2018;39(2):501–10.
47. Zheng A, Bai J, Ha Y, et al. Integrated analysis of the relation to tumor immune microenvironment and predicted value of Stonin1 gene for immune checkpoint blockage and targeted treatment in kidney renal clear cell carcinoma. BMC Cancer. 2023;23(1):135.
48. Tang YF, Qiao B, Huang YB, et al. ARPC1B is a novel prognostic biomarker for kidney renal clear cell carcinoma and correlates with immune infiltration. Front Mol Biosci. 2023;10:1202524.
49. Liu H. Expression and potential immune involvement of cuproptosis in kidney renal clear cell carcinoma. Cancer Genet. 2023;274–275:21–5.
50. Mehla K, Singh PK. Metabolic regulation of macrophage polarization in cancer. Trends Cancer. 2019;5(12):822–34.
51. van der Leun AA-O, Thommen DA-O, Schumacher TA-O. CD8(+) T cell states in human cancer: insights from single-cell analysis. Nat Rev Cancer. 2020;20(4):218–32.
52. Rosenberg SA, Yang JC, Sherry RM, Kammula US, et al. Durable complete responses in heavily pretreated patients with metastatic melanoma using T-cell transfer immunotherapy. Clin Cancer Res. 2011;17(13):4550–7.
53. Chen X, Xu R, He D, et al. CD8(+) T effector and immune checkpoint signatures predict prognosis and responsiveness to immunotherapy in bladder cancer. Oncogene. 2021;40(43):6223–34.
54. Lee SA-O, Lee YJ, Choi I, et al. CXCL16/CXCR6 axis in adipocytes differentiated from human adipose derived mesenchymal stem cells regulates macrophage polarization. Cells. 2021;10(12):3410.
55. Sun C, Mezzadra R, Schumacher TN. Regulation and function of the PD-L1 checkpoint. Immunity. 2018;48(3):434–52.
56. Anand PA-O, Guillaumet-Adkins AA-O, Dimitrova VA-O, et al. Single-cell RNA-seq reveals developmental plasticity with coexisting oncogenic states and immune evasion programs in ETP-ALL. Blood. 2021;137(18):2463–80.
57. Zhai YA-OX, Celis-Gutierrez J, Voisinne G, et al. Opposing regulatory functions of the TIM3 (HAVCR2) signalosome in primary effector T cells as revealed by quantitative interactomics. Cell Mol Immunol. 2021;18(6):1581–3.
58. Latchman Y, Wood C, Chernova T, Chaudhary D, et al. PD-L2 is a second ligand for PD-1 and inhibits T cell activation. Nat Immunol. 2001;2(3):261–8.

Publisher's Note